DIAMOND SYNTHESIS IN A 50 KW INDUCTIVELY COUPLED ATMOSPHERIC PRESSURE PLASMA TORCH

T.G. OWANO,* D.G. GOODWIN,** C.H. KRUGER,* and M.A. CAPPELLI*
*High Temperature Gasdynamics Laboratory, Department of Mechanical Engineering, Stanford University, Stanford, California.
**Division of Engineering and Applied Science, California Institute of Technology, Pasadena, California.

ABSTRACT

Polycrystalline diamond coatings have been deposited on metal substrates using a 50 kW atmospheric pressure inductively coupled plasma torch. The argon-hydrogen-methane plasma generated has a free stream active area of 35 cm^2 and a temperature of approximately 5000 K. Growth rates obtained for a highly diluted plasma are of the order of 10 μm/hour. In this work, a flat plate boundary layer flow reactor is used to generate diamond growth at a surface in a well understood fluid dynamic situation. The growth morphology is found to vary significantly with reactor processing conditions and location downstream of the leading edge. Scanning electron microscopy indicates that well faceted crystals are obtained with growth along the 100 and 111 planes. Nearly continuous films are also formed and found to be of lower quality. The results are compared to the predictions of a two-dimensional boundary layer model of the reacting flow environment. Measured and predicted growth rates show good agreement.

INTRODUCTION

High growth rate synthesis of polycrystalline diamond using atmospheric pressure plasmas is a promising alternative to low pressure synthesis techniques [1-3]. It has already been demonstrated that growth rates as high as 900 μm/hour can be achieved in direct current (DC) arcs [4-7], with a noticeable improvement in purity when compared to microwave deposited diamond film. Matsumoto et al [8] was the first to demonstrate diamond synthesis in an atmospheric pressure, electrodeless, inductively coupled plasma (ICP) discharge. Since then, there has been limited study of atmospheric pressure ICP technology for diamond synthesis, although such a plasma introduces a minimum of impurities and thus may be preferred over the DC arc in the synthesis of diamond coatings. In addition, inductively coupled plasmas may be attractive for large area applications since they can be generated over large volumes.

The study of diamond synthesis in an inductively coupled atmospheric pressure plasma is attractive for several reasons. Unlike low pressure deposition techniques, atmospheric pressure ICPs are at high enough pressure to ensure that the electron and heavy particle temperatures are essentially equal downstream of the coil region [10]. The flat plate boundary layer flow reactor also provides a situation in which the fluid dynamics are relatively well understood. Thus the flow in the free stream and within the boundary layer of a growth surface placed at sufficient distances downstream from the excitation source is complicated solely by the effects of finite rate chemistry.

In this paper, we report the results of our experimental and computational investigation of diamond synthesis in an inductively coupled plasma flow reactor. We report here primarily our results of experiments involving diamond growth on polycrystalline molybdenum. Our diamond films are grown under conditions similar to those of Matsumoto et al [8] and Koshino et al [4]. A complete parametric study is currently underway to investigate the range of optimum processing conditions, and we suspect that this range can be considerably different than that observed in the low pressure plasma enhanced chemical vapor deposition (PECVD) of diamond.

EXPERIMENTAL FACILITY

The measurements described here were conducted with a nominally 50 kW TAFA model 66 RF induction plasma torch, powered by a LEPEL model T-50 power supply. The vertical 5-coil torch has a 7.5 cm inner diameter and an inner length of 26.5 cm measured between the gas injection plate and the 7 cm exit nozzle, which is 6 cm above the upper coil. The present experiments were conducted inside a water cooled quartz test section which is shown schematically in Figure 1. The test section has an inner diameter of 7 cm and a length of 18 cm above the nozzle exit. The power supply and torch, and the test section cooling water systems, were separately instrumented with thermocouples and flowmeters to independently obtain calorimetric energy balances. These energy balance techniques have shown to be useful in characterizing the plasma [10].

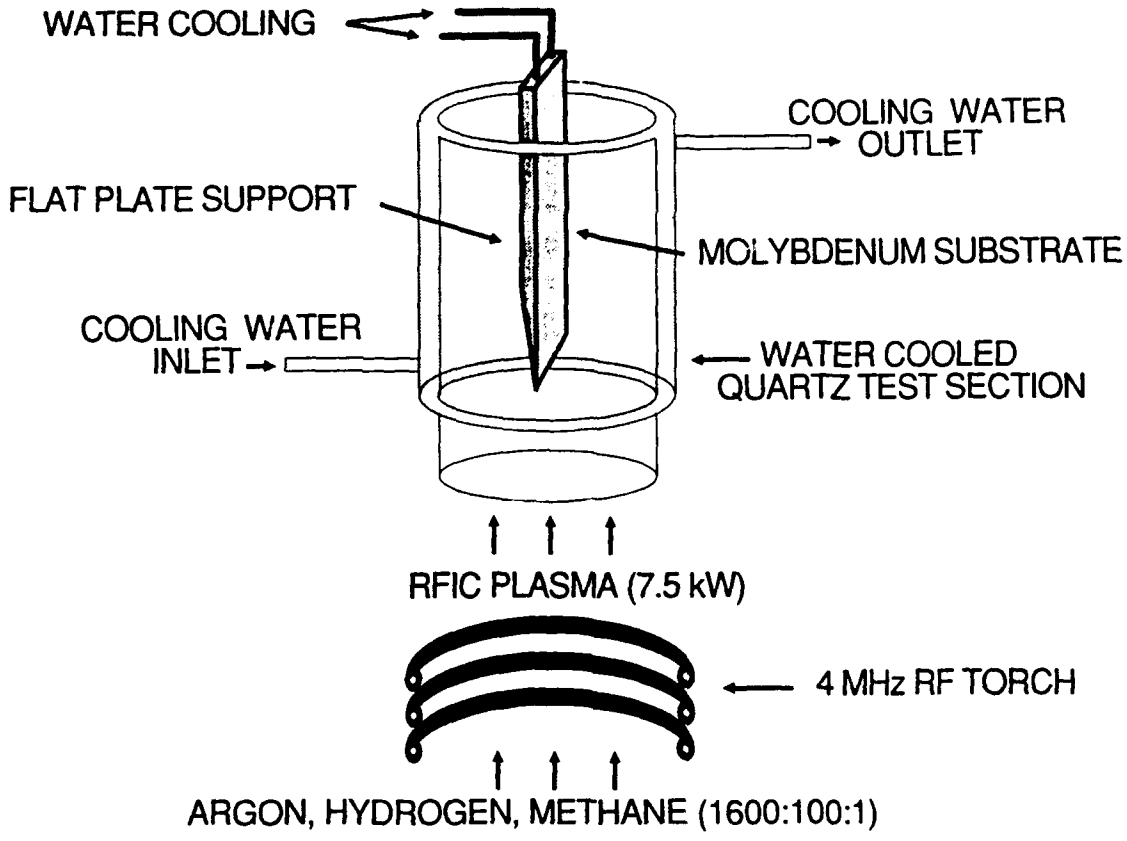

Figure 1. Schematic of flat plate boundary layer flow reactor.

Plasma emission measurements were made using a SPEX model 1400-11 3/4 meter scanning monochromator fitted with a Hamamatsu model R1104 photomultiplier tube. Absolute intensity calibrations were obtained by means of a tungsten strip lamp, with a calibration traceable to NBS standards. A 4 mirror, dual translation stage, two lens optical collection system allowed lateral and axial translational scans of the plasma emission. Data sets acquired using a Stanford Research Systems model SR510 lock-in amplifier were transferred to and stored on a laboratory computer for processing.

Substrates are supported within the quartz test section by means of a water cooled holder. The flat plate boundary layer configuration is shown schematically in Figure 1. The substrate is attached to a water cooled support and held parallel to the oncoming plasma free stream. Substrate temperature is monitored with Pyro-Micro disappearing filament optical pyrometer, modified with a narrow spectral filter centered at 632 nm to reject background plasma emission. Mixture gases (hydrogen and methane) can be added to the carrier gas (argon) before passage through the RF discharge region, or immediately after it.

REACTOR CONDITIONS

Conditions within the reactor are monitored using several methods including calorimetric energy balance, optical thermometry, and emission spectroscopy. Calorimetric energy balance of the power supply and torch yields a net deposited power of approximately 7.5 kW. Total flowrate was approximately 110 l/min with $Ar/H_2/CH_4$ ratios of 1600:100:1.

Use of a disappearing filament optical pyrometer allowed determination of the substrate "brightness" temperature during deposition. Determination of the actual substrate thermal temperature is hampered by an unknown surface emissivity of the coated substrate, but is thought to be less than approximately 100 °C above the "brightness" temperature. Measured substrate brightness temperatures varied from approximately 1150 °C near the leading edge to 900 °C far downstream.

Emission spectroscopy of the plasma, made through the quartz test section, shows a number of emitting species including C_2 (Swan bands), CH, and atomic hydrogen lines (Balmer series), as well as CN, a common impurity. Analysis of the relative and absolute emission of the

hydrogen spectral lines permitted measurement of the plasma temperature. For the conditions reported here, free stream temperatures were approximately 5000 K which is consistent with the calorimetric energy balance. Absolute emission intensity of the continuum radiation permitted determination of the electron density. Electron densities of approximately 2.0×10^{14} cm^{-3} were found throughout the flow. This value is higher than the Saha equilibrium value at the measured free stream temperature, but an elevated electron density is anticipated due to the finite electron-ion recombination rates, which control the decay from the initially high electron densities generated within the RF discharge region.

RESULTS

Inspection of the substrate after a 1 hour run duration shows growth from approximately 1 cm downstream of the leading edge to approximately 9 cm downstream. Moving downstream from the leading edge, scanning electron microscopy indicates an abrupt transition from blank molybdenum to large (25 μm) well faceted individual crystals at approximately 1 cm from the leading edge. This region transitions to a more film like growth at 2-2.5 cm from the leading edge, but becomes less faceted with approximately 3-4 μm ball like agglomerated grains. This film growth continues downstream with the grain size and film thickness decreasing to approximately 1 μm at 6 cm from the leading edge and finally disappearing altogether at approximately 9 cm from the leading edge. Continuity of the film is good, with approximately 95% coverage at most locations, although it is apparent that growth is not far enough along at this run duration for all grains to have agglomerated or begun columnar type growth. An example of the film growth is shown with a scanning electron micrograph in Figure 2.

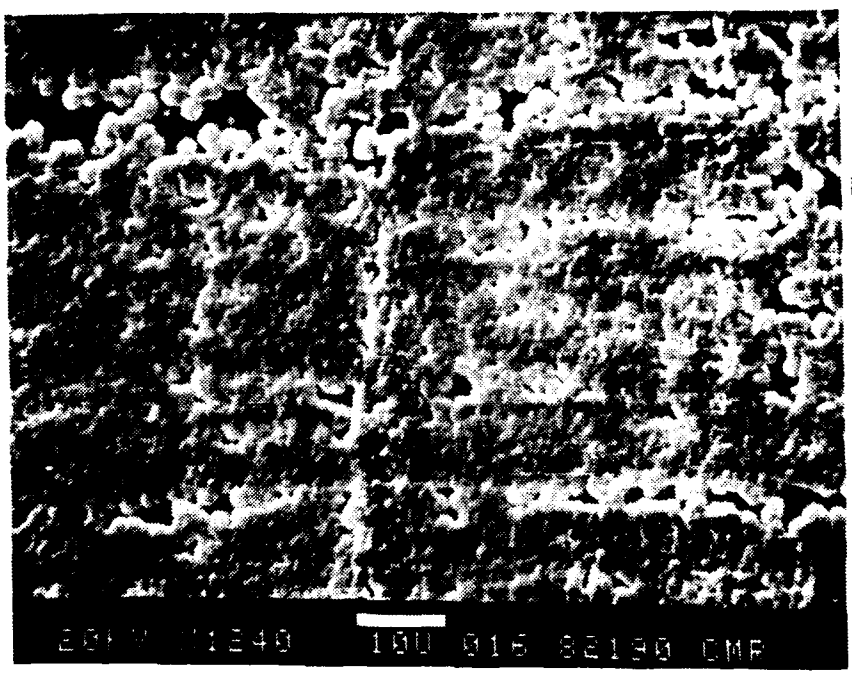

Figure 2. Scanning electron micrograph of growth at 3.5 cm from leading edge.

For comparison with results of the computational simulation of the growth rate, an effective film thickness was derived from the micrographs of the deposited film. Since the film growth had not fully agglomerated or begun columnar growth, the average grain size was taken as a measure of the film thickness and multiplied by the fractional film coverage to produce an effective film thickness at many locations.

SIMULATION

A numerical simulation of the plasma environment near the substrate has been carried out, using an upgraded version of the computational model developed previously by Goodwin [11] to simulate DC torch boundary layers. The model solves for the complete 2-D velocity, temperature, and species concentration fields in the boundary layer above the substrate, including both gas-phase and surface chemistry, and can handle cases with an axially-varying substrate temperature and an imposed pressure gradient.

To model the present experiments, the gas-phase species considered are Ar, H_2, H, and all C_1 and C_2 hydrocarbons, for a total of 15 species. The gas-phase reaction mechanism consists of 31 elementary reactions, most of which are taken from the mechanism used by Goodwin and Gavillet [12] to model hot-filament diamond growth. In fact, the predicted species concentrations are not very sensitive to the details of the mechanism, since, as discussed below, the plasma is nearly in chemical equilibrium beyond a few millimeters from the substrate. Close to the substrate, the H superequilibrium is large, but even here most bimolecular reactions are in partial equilibrium.

The surface reactions responsible for diamond growth do not appreciably affect the gas-phase concentration profiles, since the measured rates indicate that these reactions are kinetically limited. These reactions are therefore decoupled from the gas-phase, and diamond growth rates may be solved for after the species concentrations at the surface are determined.

However, radical recombination on the surface may significantly alter the species concentrations near the surface. This is particularly important for H atoms, since there is no mechanism to regenerate H lost through recombination, in contrast to hydrocarbon radicals, which will be regenerated by gas-phase H-abstraction to maintain partial equilibrium with H and H_2. Thus, any model of the gas phase should include H atom recombination on the surface.

H atom surface recombination is calculated using the following simplified picture: we assume that the surface consists of (111) diamond, and thus there are 1.8×10^{15} surface atoms per cm^2. We assume that H reacts with the surface via the two reactions :

$$H^{gas} + \text{C-H} \rightleftharpoons H_2^{gas} + C^{\bullet} \qquad (1)$$

$$H^{gas} + C^{\bullet} \rightleftharpoons \text{C-H} \qquad (2)$$

where C-H represents an adsorbed surface H, and $C^{\bullet}$ a dangling surface bond. Reactions (1) and (2) together represent a mechanism for catalytic recombination of H. The reaction rate constant for reaction (1) is taken from Westbrook et al. [13] for H-abstraction from a tertiary carbon, and the rate constant for (2) is set to 1.0×10^{14} $mol^{-1}cm^3s^{-1}$ [14]. These values are probably upper bounds, since they are values appropriate for gas-phase reactions, and do not account for the steric hindrances which may be significant on the surface. We calculate rate constants for the reverse reactions from detailed balance, using estimated values for $\Delta G^0(T)$ (-18.5 kcal/mol and -54.9 kcal/mol for reactions (1) and (2) respectively, at 1200 K). For the H and H_2 concentrations we calculate at the substrate, this recombination mechanism is equivalent to an effective H-atom surface recombination probability varying from 0.25 at 1200 K to 0.39 at 1475 K. The substrate boundary condition used for the H and H_2 species equations is that the net creation rate at the surface due to surface reactions (1) and (2) equals the flux away from the surface due to diffusion and convection; for all other species, the surface boundary condition is that the diffusion velocity at the surface is zero.

To model the experimental conditions, we take a freestream temperature of 5000 K, a freestream velocity of 820 cm/s, and assume that the plasma is in chemical equilibrium outside the boundary layer. The plasma elemental composition corresponds to the initial 1600:100:1 $Ar/H_2/CH_4$ ratio. The measured substrate temperature profile is used, which varies from 1475 K at the leading edge to 1183 K at 10 cm downstream. A significant limitation of the simulation is that only neutral species are included, and no account is taken of plasma effects. As long as the electron temperature equals the heavy particle temperature, as is generally the case for such plasmas, electron-induced chemistry will be minor. However, it is possible that $T_e > T$ in the boundary layer where temperature gradients are large, which might induce chemistry not included in the present model.

The calculated temperature profile and several mole fraction profiles are shown in Figure 3 for an axial distance 4 cm from the leading edge, which is in the middle of the region where continuous growth is observed. For these conditions, the thermal boundary layer thickness is roughly 1 cm. The shoulder in the temperature profile at 0.3 cm results from heating due to H recombination.

The mole fraction profiles shown in Figure 3b indicate some of the effects of chemistry occurring on and near the substrate. H atoms are strongly depleted at the surface ($X_H(0) = 5.4 \times 10^{-5}$), due both to surface and gas-phase recombination. For these conditions, the H

concentration at the surface is diffusion limited, and therefore inversely proportional to the recombination probability.

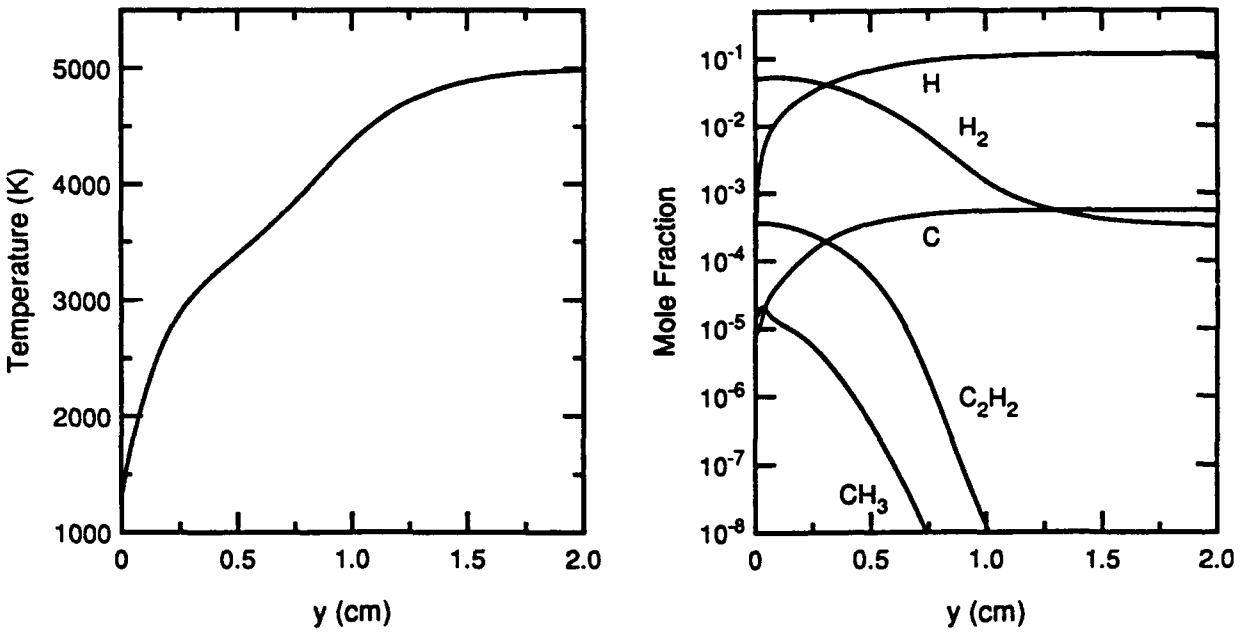

Figure 3. Calculated temperature and selected mole fraction profiles at x = 4 cm.

Beyond approximately 0.5 cm from the substrate, all gas phase reactions are nearly equilibrated, and thus the plasma is close to local chemical equilibrium. Closer than 0.5 cm, significant non-equilibrium occurs, particularly for three-body recombination reactions. Many bimolecular reactions, however, remain in partial equilibrium to within tens of microns from the substrate surface. This is responsible for the feature shown in the CH_3 profile near the surface: as the H concentration decreases rapidly near the substrate due to surface recombination, the hydrocarbon radical populations attempt to adjust to maintain partial equilibrium. Thus, to a good approximation the hydrocarbon populations are tightly coupled to the local H and H_2 concentrations, and the most important factor determining the gas composition is the recombination of H in the gas and on the surface.

We have calculated diamond film growth rates using our predicted surface concentrations of H, H_2, and CH_3 together with the diamond growth mechanism of Harris [14], using the rate constants for the "dense" case of Ref. [14]. Since growth under these conditions is kinetically-limited, these surface reactions do not affect the gas-phase concentrations, and the growth rate calculation may be decoupled from the gas-phase model.

The growth rate calculated in this manner is shown as the solid curve in Figure 4. The calculated rate is within a factor of two of the measured rate, and reproduces the fall-off with axial distance. The model does not predict the sudden onset of nucleation at 1 cm, or the sudden drop at 9 cm. These features may be due to nucleation phenomena, which fall outside the scope of the homoepitaxial growth mechanism of Ref. [14]. Considering the uncertainties associated with the experiment, the model, and the proposed growth mechanism, the agreement is better than expected, and may be to some extent fortuitous. Nevertheless, it is worth pointing out that no adjustable parameters enter into the calculation.

The dashed curve in Figure 4 indicates the sensitivity of the predicted growth rate to the H-atom surface recombination rate coefficient. This curve was calculated with the rate constants for reactions (1) and (2) arbitrarily reduced by a factor of two. Since the surface H concentration scales inversely with the recombination rate coefficient, and the assumed growth mechanism is approximately first-order in [H], this results in a nearly doubled growth rate. These calculations indicate that for this environment H-atom surface recombination may be a significant factor determining the film growth rate.

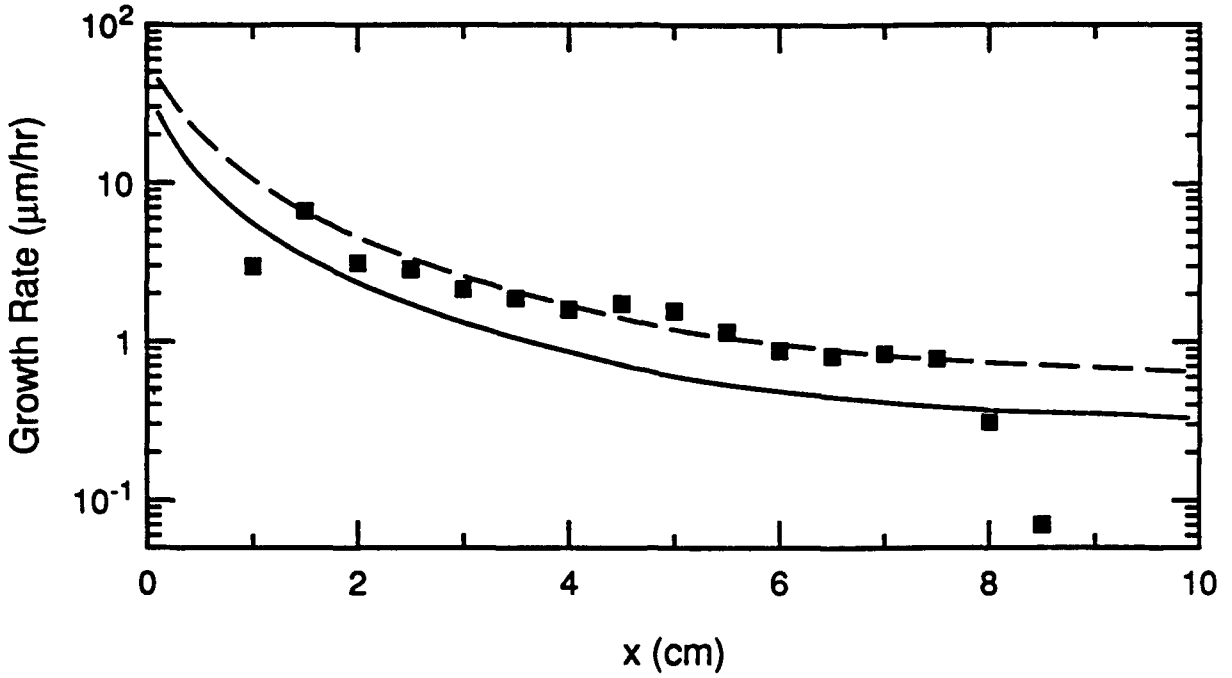

Figure 4. Growth rate vs. distance from leading edge.

CONCLUSIONS

Large area polycrystalline diamond coatings have been deposited with relatively large growth rates using an atmospheric pressure inductively coupled plasma. A well-defined flat-plate boundary layer flow was employed to facilitate numerical simulation of the experiment. Good agreement was obtained between the calculated and measured diamond growth rates, and the simulations indicate a sensitivity of the growth rate to H recombination on the surface. Although the growth rates for the present highly diluted gas stream are low, the technique is well suited for scale-up to much higher methane flowrates, and correspondingly higher growth rates. Experimental and computational work on high-rate synthesis in this reactor is currently in progress.

REFERENCES

1. F.P. Bundy, H.T. Strong, and R.H. Wentorf Jr., Nature **176**, 51 (1955)
2. H. Liander and E. Lundblad, Arkiv. Kemi. **16**, 139 (1960).
3. P.S. DiCarli and J.C. Jamieson, Science **133**, 182 (1961).
4. N. Koshino, K. Kurihara, M. Kawarda, and K. Sasaki, Extended Abstracts from the Spring Meeting of the Materials Research Society (Materials Research Society, Pittsburgh, PA), p.85, April 5-9, Reno, Nevada (1988).
5. S. Matsumoto, Extended Abstracts from the Spring Meeting of the Materials Research Society (Materials Research Society, Pittsburgh, PA), p. 119, April 5-9, Reno, Nevada (1988).
6. F. Akatsuka, Y. Hirose and K. Komaki, Jap. Journal of Appl. Phys. **27**, L1600 (1988).
7. N. Ohtake and M. Yoshikawa, Journal of the Electrochemical Society **137**, (1990).
8. S. Matsumoto, H. Hino and T. Kobayashi, Appl. Phys. Lett. **51**, 737 (1987).
9. M. Mitchner and C.H. Kruger, *Partially Ionized Gases* (J. Wiley and Sons, New York, 1973), p. 47.
10. T.G. Owano, M.H. Gordon and C.H. Kruger, to appear in Phys. Fluids B; Plasma Physics, Dec. 1990.
11. D.G. Goodwin, in *Technology Update on Diamond Films*, edited by R.P.H. Chang, D. Nelson, and A. Hiraki (Mater. Res. Soc. Extended Abstracts EA-19, Pittsburgh, PA 1989) pp. 153-156.
12. D.G. Goodwin and G.G. Gavillet, J. Appl. Phys. (in press).
13. C.K. Westbrook, J. Warnatz, and W.J. Pitz, in Proc. Twenty-Second Symposium (International) on Combustion, P. 893, The Combustion Institute, Pittsburgh, PA (1988).
14. S.J. Harris, Appl. Phys. Lett. **56**, 2298 (1990).